

KTH ROYAL INSTITUTE OF  
TECHNOLOGY

SD2155 FLOW ACOUSTICS

PROJECT ASSIGNMENT 2021

---

## Analysis of a Truck Muffler

---

*Group:* 11

*Name:* Fang, Siye

Wang, Yuhao

Wong, Cho Hang Jonathan

*Date:* March 5, 2021

# Contents

<b>1</b>	<b>Introduction</b>	<b>1</b>
<b>2</b>	<b>Measurement</b>	<b>1</b>
2.1	Set-up . . . . .	1
2.1.1	Two-port data . . . . .	1
2.1.2	Flow noise data . . . . .	2
2.2	Two-microphone method . . . . .	3
2.3	Results . . . . .	6
<b>3</b>	<b>Simulation</b>	<b>9</b>
3.1	SIDLAB model . . . . .	9
3.2	Comparison between measured and simulated data . . . . .	10
3.3	Model tuning . . . . .	11
3.4	Insertion loss optimization . . . . .	13
3.4.1	IL at lab conditions and real operating schemes . . . . .	14
3.4.2	Optimised tailpipe length . . . . .	14

# 1 Introduction

In this project, a modern truck silencer from SCANIA was studied experimentally and by two-port simulation. The experiment determines two-port data for further simulation, and self-generated noise data. Based on the experiment data, a simulation model was built on SIDLAB to study transmission loss and insertion loss between the model and experimental data, as well as “tailpipe” length for optimal noise attenuation.

Because of the current restrictions, laboratory exercise was cancelled and data was pre-recorded for post-processing.

## 2 Measurement

### 2.1 Set-up

#### 2.1.1 Two-port data

To obtain the two-port data, the muffler was mounted in the rig shown in figure 1<sup>1</sup> and tested for its transmission function to determine its T-matrix in the two-port model. Tests were performed at cold conditions (20°C) and no flow.

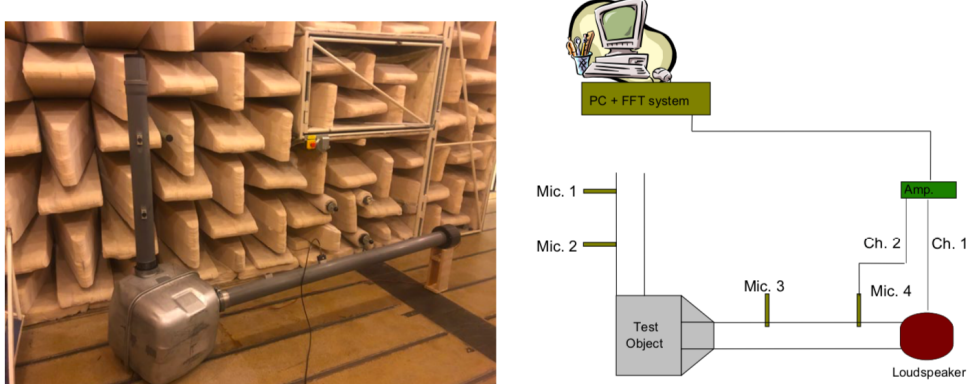


Figure 1: Set-up of muffler rig in the MWL laboratory for 2-port data measurement, and drawing of measurement arrangement.

Two acoustic states are needed to solve the two-port problem, which will be further elaborated in section 2.2, and two-load technique was used to achieve the

---

<sup>1</sup> Figures taken from lab menu.

different states. The two-load technique employs a single source at one end, in our case a loudspeaker at the upstream end of the muffler; and two different plugs on the other end, in our case a rigid end for almost complete reflection termination and a porous plug for reflection-free termination.

To determine sound pressure and volume velocity, we perform wave decomposition using the two-microphone technique. As shown in figure 1, we have two microphone positions upstream and two downstream, all at known positions. However, in our case, instead of two microphones a single microphone was used and moved between the four different positions to avoid microphone calibration.

During measurement, white noise generated by the Fourier system was fed to a power amplifier, which drives the loudspeakers to provide a sound source. Transfer function between voltage supplied to the loudspeaker and voltage output from the microphone was measured, instead of the raw pressure data from microphone, so as to reduce the effect of background acoustic or electric noise. For the four microphone positions and two loads, a total of 8 measurements were taken.

### 2.1.2 Flow noise data

Flow through a muffler generates self-noise due to flow separation. To characterize this noise sound power radiated from muffler opening at different flow speeds was measured.

The experiment setup is shown in figure 2. The muffler is mounted to a wall in the reverberation room in MWL, and its inlet is connected to a fan on the other side of the wall in the anechoic chamber, which pressurises the muffler and generates flow.

Sound power was determined according to the ISO 3741 standard, which compares sound pressure of the muffler to that of a known source. The source used is a B&K reference sound power source. A rotating microphone captures the pressure in the room for better sound pressure average. The microphone samples pressure at 16 kHz for 32 averages, which takes the same time for it to complete two revolutions. Flow velocity and pressure drop were measured by a pitot tube and

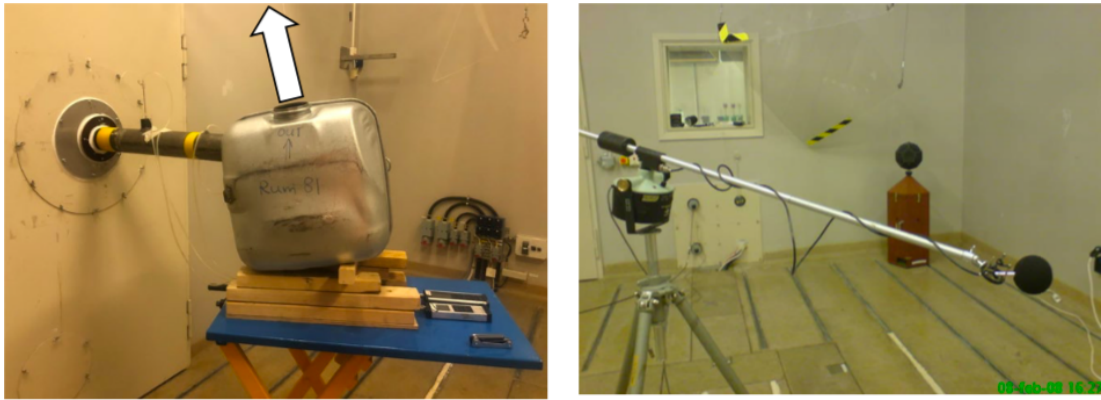


Figure 2: Setup for flow noise measurement in MWL

pressure gauge respectively at the muffler inlet. Three velocities, 10.3, 20.5 and  $39.0 \text{ ms}^{-1}$ , were tested for.

In addition to flow velocity, presence of a “tailpipe” affects noise generation. Tests were made with and without a tailpipe for each flow velocity.

7 sets of data were taken in total, one for the reference source, 6 in total for each velocity with and without tailpipe.

## 2.2 Two-microphone method



Figure 3: An acoustic 2-port.

The muffler is modeled as an acoustic 2-port, with pressure  $p$  and volume velocity  $q$  as state variables. Using the transfer matrix formulation, the system equation

is given by

$$\begin{pmatrix} \hat{p}_a \\ \hat{q}_a \end{pmatrix} = \underbrace{\begin{pmatrix} T_{11} & T_{12} \\ T_{21} & T_{22} \end{pmatrix}}_{\mathbf{T}} \begin{pmatrix} \hat{p}_b \\ \hat{q}_b \end{pmatrix}. \quad (1)$$

The state variables are measured to solve for entries in transfer matrix  $\mathbf{T}$ . Since there are 4 matrix entries, 4 equations are needed to determine  $\mathbf{T}$ . This can be done by testing the 2-port under two different acoustic states. There are two methods to create the two states:

- Two-load: A single source is placed on one end, and measurements are done for two different terminations on the other end.
- Two-source: Measurements are done for a source placed on one end, and then on the other end.

As mentioned in the previous section, the two-load method is used in this project.

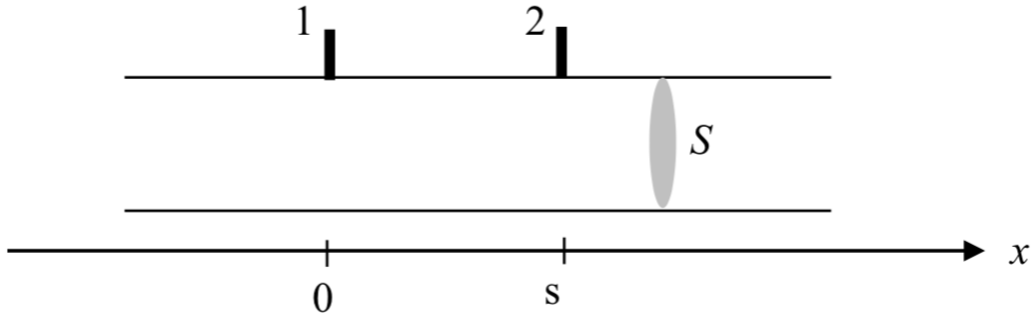


Figure 4: Placement of 2 microphones on inlet or outlet duct.

To determine the state variables, one can use a microphone to measure pressure and a special probe to measure velocity. Or, one can use the *two-microphone method* to measure pressure at two known positions on the inlet and outlet duct, then perform wave decomposition to obtain flow velocity. Figure 4 presents the experimental layout using the two-microphone method.

From the lab menu, pressures at the two microphone positions in figure 3 are

$$\begin{cases} \hat{p}_1 &= \hat{p}_+ + \hat{p}_- \\ \hat{p}_2 &= \hat{p}_+ e^{-ik_+ s} + \hat{p}_- e^{ik_- s}, \end{cases} \quad (2)$$

where  $\hat{p}_+$ ,  $\hat{p}_-$  are the travelling wave amplitudes, and the wave numbers are given by  $k_{\pm} = \frac{\omega/c_0}{1 \pm M}$ , which  $M$  is the Mach number. Solving for the travelling wave amplitudes, we have

$$\begin{cases} \hat{p}_+ &= D^{-1}(\hat{p}_1 e^{ik_- s} - \hat{p}_2) \\ \hat{p}_- &= D^{-1}(-\hat{p}_2 e^{ik_+ s} + \hat{p}_1), \end{cases} \quad (3)$$

where  $D = e^{ik_- s} - e^{ik_+ s} = 2i \exp(\frac{iMk_0 s}{1-M^2}) \sin(\frac{k_0 s}{1-M^2})$  and  $k_0 = \omega/c_0$ . Thus, the two-microphone method produces a wave decomposition as long as

$$\frac{k_0 s}{1 - M^2} \neq n \cdot \pi, \quad n = 0, 1, 2 \dots$$

The best accuracy is around  $k_0 s / (1 - M^2) = \pi/2$ , and for practical application the frequency range should be used in

$$0.1\pi \leq \frac{k_0 s}{1 - M^2} \leq 0.8\pi, \quad (4)$$

according to an investigation by Åbom and Böden.

Rewriting equation 3 in terms of frequency response functions  $H$  using voltage  $e$  as reference, and referring the amplitudes at an arbitrary position we have

$$\begin{cases} H_{p+,2}(x) &= D^{-1}(H_{p1,e} e^{ik_- s} - H_{p2,e}) \\ H_{p-,2}(x) &= D^{-1}(-H_{p1,e} e^{ik_+ s} + H_{p2,e}). \end{cases} \quad (5)$$

Further operation gives the pressure and velocity transfer functions  $H_{p,e}$  and  $H_{q,e}$

$$\begin{cases} H_{p,e}(x) &= H_{p+,e}(x) + H_{p-,e}(x) \\ H_{q,e}(x) &= (H_{p+,e}(x) - H_{p-,e}(x)) \frac{S}{\rho_0 c_0}. \end{cases} \quad (6)$$

## 2.3 Results

The transmission loss obtained with measured data is as follows.

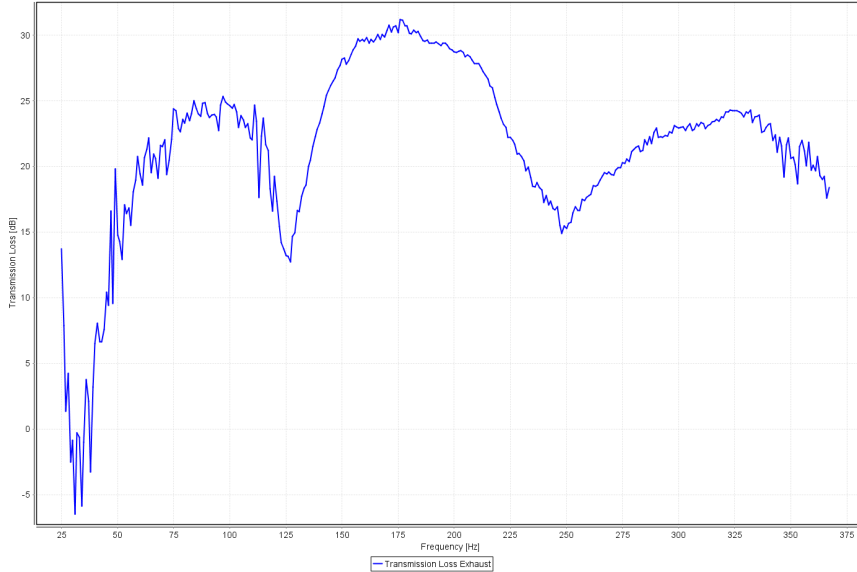


Figure 5: Transmission loss as a function of frequency.

Plots for self-noise measurements are as follows.

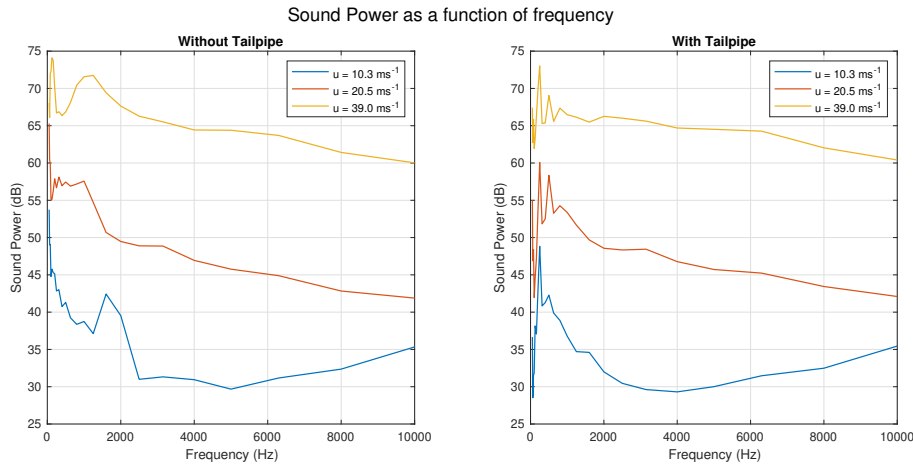


Figure 6: Measured sound power level as function of frequency.

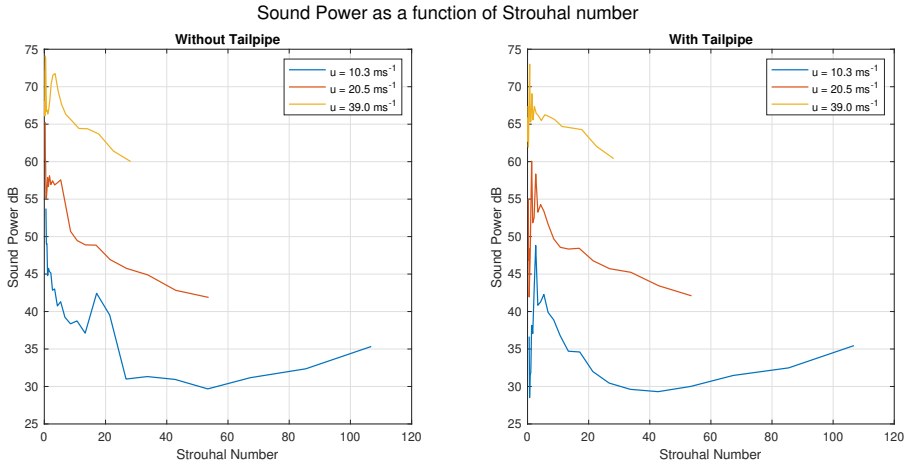


Figure 7: Measured sound power level as function of Strouhal number.

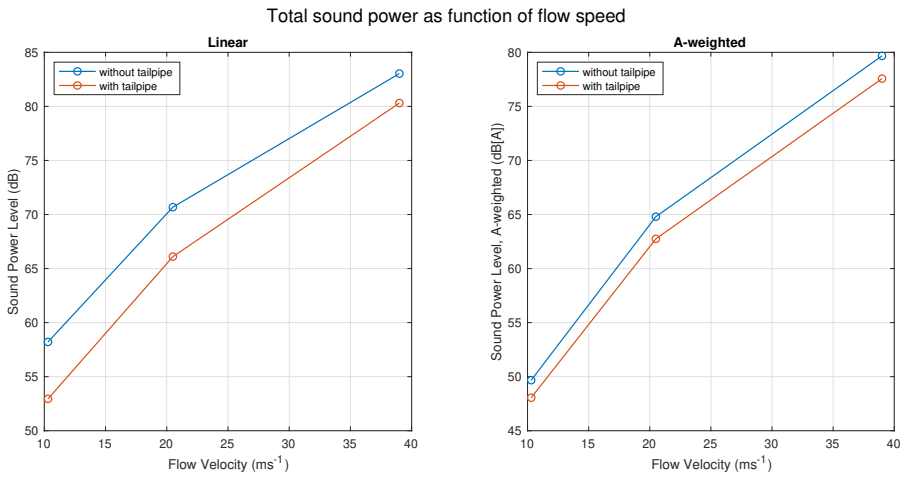


Figure 8: Total sound power as function of mean flow speed.

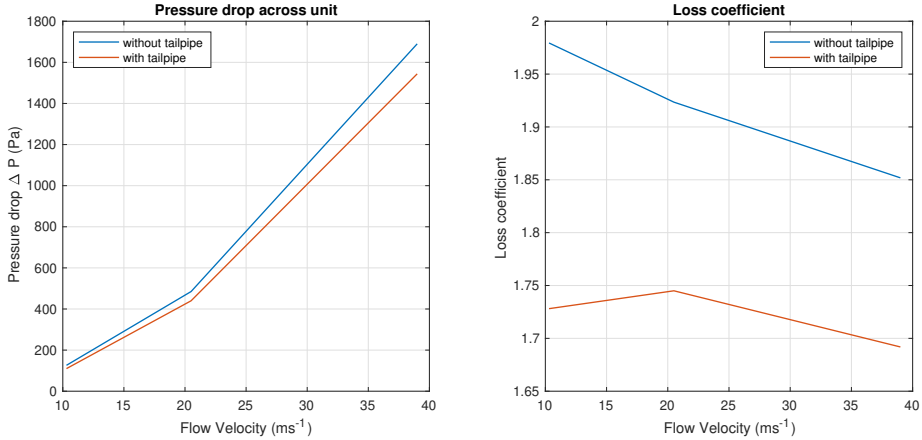


Figure 9: Pressure drop and Loss coefficient as a function of mean flow speed.

From the plots, we see that there is stronger noise, i.e. larger sound power, when flow velocity is higher. With higher flow velocity, there is stronger flow separation and naturally it is noisier.

It is noted that pressure drop increases with flow velocity. Because of the stronger flow separation at higher speeds, more pressure is needed to drive the flow. Also, since damping increases with speed, there is stronger resistance when flow velocity is higher, hence the increasing pressure drop.

From figure 8, we see that a tailpipe reduces flow noise. The tailpipe also moved resonant frequencies between 1.5 kHz and 2 kHz to below 1 kHz, as shown figure 6 and 7. Also, the tailpipe lowers the both pressure drop across the unit and loss coefficient.

Pressure drop  $\Delta P$  is presented in table 1 alongside with the loss coefficient  $C_L$ , which is given as  $C_L = \frac{\Delta P}{\frac{1}{2} \rho_0 U^2}$ .

Flow Velocity (ms <sup>-1</sup> )	$\Delta P_{\text{no tailpipe}}$ (Pa)	$C_{L,\text{no tailpipe}}$	$\Delta P_{\text{with tailpipe}}$ (Pa)	$C_{L,\text{with tailpipe}}$
10.3	125	1.9795	110	1.7281
20.5	485	1.9235	440	1.7450
39.0	1690	1.8519	1544	1.6919

Table 1: Pressure drop and loss coefficient at different speeds, with and without tailpipe.

### 3 Simulation

#### 3.1 SIDLAB model

The Scania truck muffler is shown in figure 12, and its corresponding SIDLAB model in figure 11,

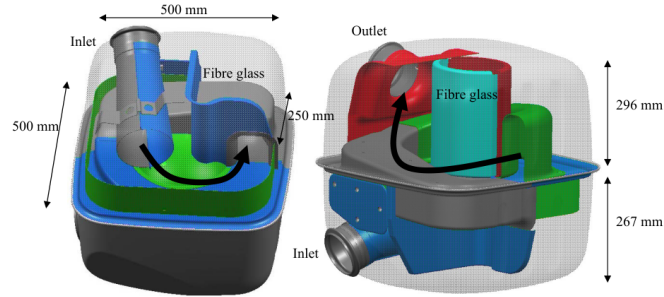


Figure 10: Truck muffler geometry.

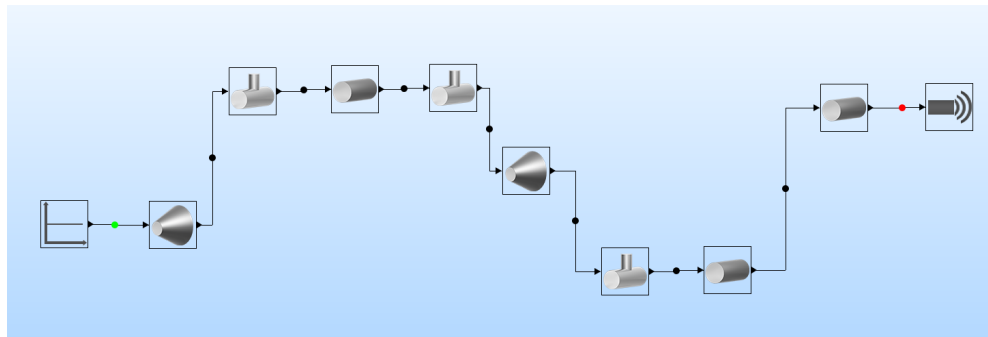


Figure 11: Sidlab model.

To model the inlet cone and spiral pipe, diffuser blocks were used in SIDLAB. Quarter-wave resonators were placed according to the hinted muffler layout shown in figure 12.

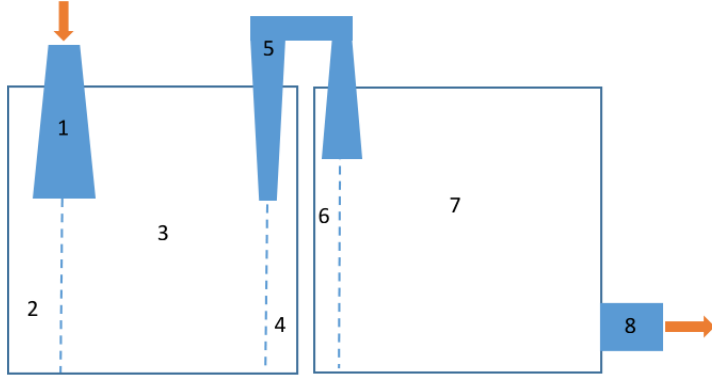


Figure 12: Hinted muffler layout

A preliminary was made in SIDLAB according to the given dimensions. Table 2 shows the initial model parameters.

Component	Length [m]	Area [ $m^2$ ]
1	0.36	$A_{in}=0.0095, A_{out}=0.0161$
2	0.1	0.1
3	0.35	0.1
4	0.05	0.1
5	1.45	$A_{in}=0.0075, A_{out}=0.0119$
6	0.05	0.11
7	0.45	0.11
8	0.1	0.0095

Table 2: Initial element dimensions.

### 3.2 Comparison between measured and simulated data

First, transmission loss (TL) was used to verify the SIDLAB model. Comparison between the model with the measured data is shown in figure 13.



Figure 13: Transmission loss of simulated muffler model and measured data.

There is significant difference in amplitude between the measured and simulated TL, but shape and extrema locations matches well below 225 Hz. The difference in amplitude may stem from the defects in the duct wall and quarterwave resonators, and mismatch of inner dimensions not specified in the project description. As the maximum deviation is larger than 3dB, the SIDLAB model was tuned to fit measured data better.

### 3.3 Model tuning

The following strategies were used to alter the model for better fit:

1. Modifying the element length  $L$ ,
2. Modifying the element area  $S$ .

In a 2-port model, as mentioned in equation 1, the transfer-matrix  $\mathbf{T}$  for a passive straight duct element is

$$\mathbf{T} = e^{-ikML/(1-M^2)} \begin{bmatrix} \cos(kL/(1-M^2)) & iZ \sin(kL/(1-M^2)) \\ (i/Z) \sin(kL/(1-M^2)) & \cos(kL/(1-M^2)) \end{bmatrix}, \quad (7)$$

where  $k = \omega/c$ ,  $Z = \rho c_0/S$ .

Assuming  $c \ll c_0$ ,  $M \rightarrow 0$ , we then get

$$\mathbf{T} = \begin{bmatrix} \cos(kL) & i\rho c_0 \sin(kL)/S \\ (iS/\rho c_0) \sin(kL) & \cos(kL) \end{bmatrix} \quad (8)$$

Altering  $L$  and  $S$  changes the transfer matrix  $\mathbf{T}$ , which ultimately changes transmission loss of the system, hence justifying the used measures. While adjusting the values, care was taken that the total volume of the chamber remained constant.

Adjustments to the model are laid out in table 3. Elements 1,5 and 8 remain unchanged. Unless otherwise stated, area or length remains the same as the original model.

Pipe NO.	Original		Case 1		Case 2		Case 3		Case 4	
	Area	Length	Area	Length	Area	Length	Area	Length	Area	Length
2	0.1	0.1	0.3	0.25	0.12	0.16	0.295	0.11		
3	0.1	0.35	0.15	0.25	0.1	0.2	0.17	0.3		
4	0.1	0.05	0.04	0.11	0.06	0.03	0.065	0.07		
6	0.11	0.05	0.07	0.1	0.04	0.1	0.05	0.1		
7	0.11	0.45	0.04	0.3	0.12	0.5	0.03	0.4		

Table 3: Pipe dimensions for four simulations. Area in  $m^2$  and length in  $m$ .

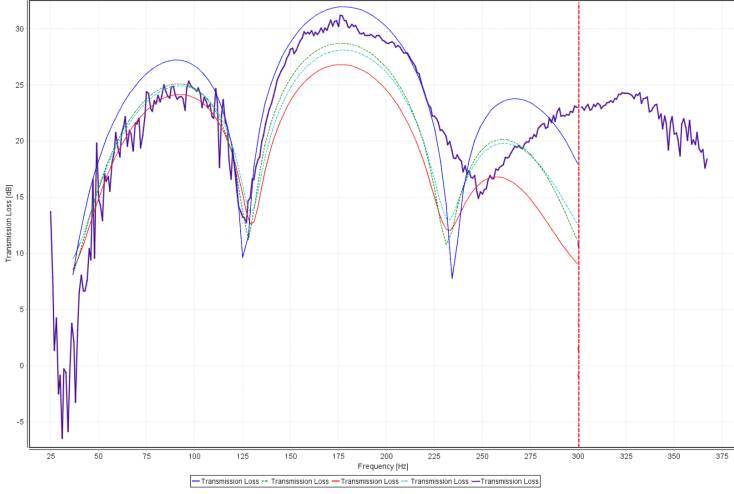


Figure 14: Comparison between of measured transmission loss and four adjusted models.

Figure 14 shows the transmitted loss of the adjusted models compared to the measured data. The red, deep blue , green and light blue curves correspond to cases 1 to 4 respectively. Of all attempts, the green curve, i.e. case 3, fits the measured data best. However to reach the final peak at around 300Hz, non of the adjustments showed good approximation. After further trials, fitting the third peak will inevitably sacrifice the accuracy for fitting the first two peaks, which is not practical. Considering that we aim to maximize the attenuation (the insertion loss IL) in the range 50-200 Hz using this model, this error can be neglected temporarily.

### 3.4 Insertion loss optimization

Based on the on the adjusted model, insertion loss (IL) for the muffler at the 50-200Hz range was evaluated. As per the project description, a free space 1-port element was used at the termination to model an open pipe termination at free space. As for the source a 1-port IC-engine with impedance  $0.7 - 0.7i$  was chosen.

### 3.4.1 IL at lab conditions and real operating schemes

The plots for insertion loss at  $20^{\circ}\text{C}$  and  $300^{\circ}\text{C}$  are presented in figure 15.

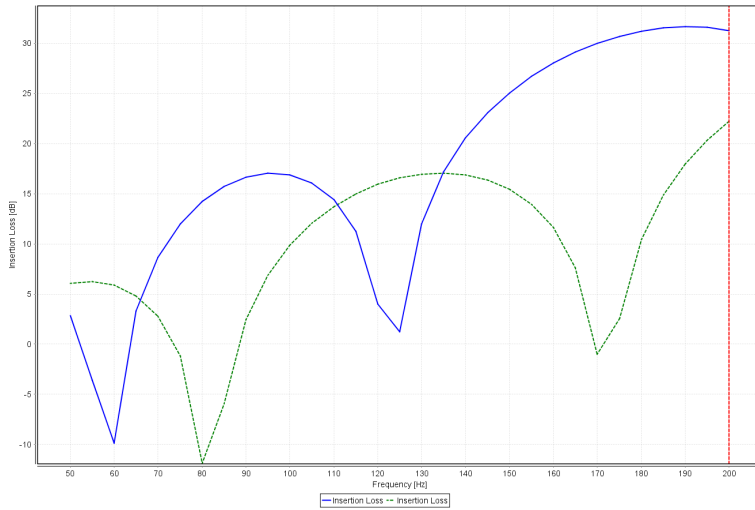


Figure 15: Insertion loss for in-lab and real life conditions.

The blue curve represents the insertion loss of lab condition at  $20^{\circ}\text{C}$ , while the green curve represents the real condition at  $300^{\circ}\text{C}$ . With the increase of temperature, the plot seems to be “shifted” right, maxima and minima occur at higher frequencies. Since speed of sound increases with temperature, and cut on frequencies  $f^c$  related to speed of sound by  $f^c \propto c_0$ , raised temperature causes raised cut-on frequencies in the same system. Thus, the plot “shifts” right. Also, the peak amplitudes of the plot decrease with temperature.

### 3.4.2 Optimised tailpipe length

To optimise this system for low frequencies, adding a tailpipe reduces the resonance and increases the "acoustic mass", considering the muffler and air as a mass-air system. Under the critical range  $50 - 200\text{Hz}$  with tailpipes with lengths between  $0.3 - 1.5\text{m}$  attached to the silencer, the insertion loss (IL) for the modified muffler is shown in figure 16.

From the figure, the optimal length that maximizes attenuation in range  $50 - 200\text{Hz}$  is approximately  $0.8\text{m}$ .

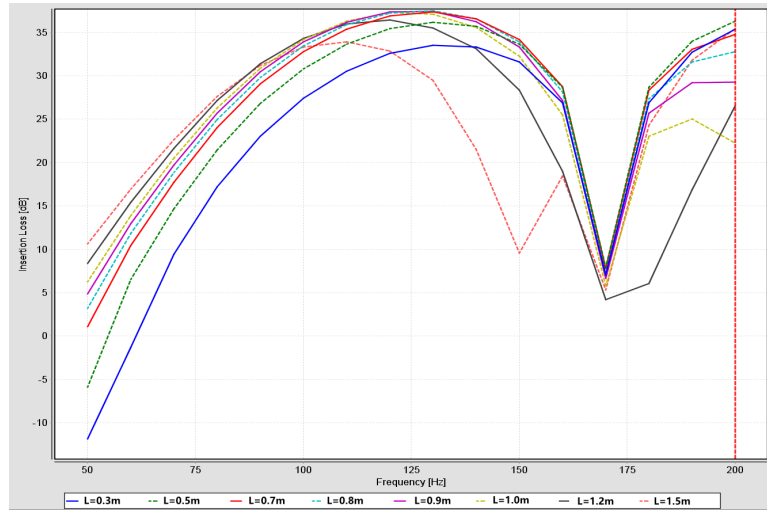


Figure 16: Insertion loss for various tailpipe lengths.

Trade-offs of using tailpipes include resonance of the pipe, which weakens the ability of the muffler as an attenuator, and added weight and volume. For the particular case when the wavelength of sound is four times as the tailpipe length, the end pipe resonance may become evident due to the weakened mass-spring resonance ability.

On designing tailpipe length, a longer tailpipe provides better attenuation, but as length increases its resonance frequency decreases, which weakens its effect in the low frequency region we aim to cure. This is particularly pronounced for the 1.2 m and 1.5 m case in figure 16. Hence, one needs to trade attenuation to maintain a high enough tail-pipe resonant frequency such that insertion loss is ideal over the concerned frequency range.

## Reference

1. *SD2155 Flow Acoustics - Project assignment 2020.*
2. *Experimental Investigation of a Truck Muffler.*